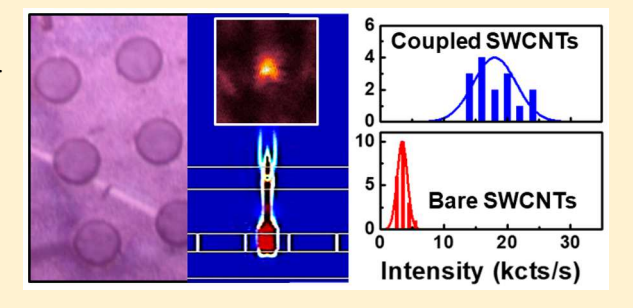


Broadband Light Collection Efficiency Enhancement of Carbon Nanotube Excitons Coupled to Metallo-Dielectric Antenna Arrays

Kamran Shayan, † Claire Rabut, † Xiaoqing Kong, ‡ Xiangzhi Li, † Yue Luo, † 6 Kevin S. Mistry, § Jeffrey L. Blackburn, So Stephanie S. Lee, and Stefan Strauf*,

Supporting Information

ABSTRACT: The realization of on-chip quantum networks ideally requires lossless interfaces between photons and solid-state quantum emitters. We propose and demonstrate on-chip arrays of metallo-dielectric antennas (MDA) that are tailored toward efficient and broadband light collection from individual embedded carbon nanotube quantum emitters by trapping air gaps on chip that form cavity modes. Scalable implementation is realized by employing polymer layer dry-transfer techniques that avoid solvent incompatibility issues, as well as a planar design that avoids solid-immersion lenses. Cryogenic measurements demonstrate 7-fold enhanced exciton intensity when compared to emitters located on bare



wafers, corresponding to a light collection efficiency (LCE) up to 92% in the best case (average LCE of 69%) into a narrow output cone of $\pm 15^{\circ}$ that enables a priori fiber-to-chip butt coupling. The demonstrated MDA arrays are directly compatible with other quantum systems, particularly 2D materials, toward enabling efficient on-chip quantum light sources or spin-photon interfaces requiring unity light collection, both at cryogenic or room temperature.

KEYWORDS: metallo-dielectric antenna, carbon nanotubes, excitons, microcavity, light collection efficiency, quantum emitter

riangle emiconducting single-walled carbon nanotubes (SWCNTs) have gained renewed interest as emitter materials for quantum photonic devices, 1,2 particularly due to the recent observation of room-temperature single photon emission in oxygen functionalized SWCNTs.³ SWCNTs are also promising absorbers and emitters in applications including solar energy conversion,⁴ and biological imaging.⁵ A drawback, however, is the limited optical quantum yield (QY) from SWCNTs that remains rather low $(2-7\%)^{6,7}$ leading to limitations for the achievable brightness of optoelectronic devices that are based on exciton emission. A direct route to improve QY can be achieved by coupling the emitter to an optical cavity mode and utilizing the Purcell effect,8 with recent findings for SWCNT excitons in high-Q dielectric cavities of QY = 12%9 and up to 64% with plasmonic nanocavities. 10 Coupling emitters to high-Q cavities that support only a narrow frequency band is nevertheless difficult to achieve at scale, particularly given the large variety of exciton emission frequencies for SWCNTs with varying chirality.11

Alternative approaches focus on improving the broadband LCE from embedded dipole emitters such as immersion lenses, 12,13 planar microcavities, 14 tip-enhanced emission from optical antennas, 15 or by fiber-taper coupling. 16 By far, the highest efficiency of any system supporting broadband coupling was achieved using carefully designed metallo-dielectric antennas (MDAs) with reported single quantum dot or single molecule LCE reaching 96–99%. 17–20 Another important aspect when collecting light from a one-dimensional (1D) dipole emitter like a SWCNT is the lateral orientation with respect to the cavity mode, which requires orientational control for plasmonic approaches. 10 In contrast, MDA cavities have been shown theoretically to support dipole emitters with arbitrary dipole orientation.¹⁹ Despite their promising optical properties, MDAs have not yet been applied for efficient light harvesting from SWCNTs.

Here we design and demonstrate on-chip MDA arrays that are tailored to collect the exciton emission from 1D SWCNTs with large LCE over a broad wavelength range covering several chiralities. Our fabrication approach involves polymer layer transfer via dry-stamping, typically utilized for assembling 2D materials, 21 to realize suspended polymer layers that trap air gaps on-chip forming the MDA. Since the entire structure is planar, the need for fabricating curved immersion lenses that were previously proposed is eliminated.¹⁹

Received: August 23, 2017 Published: December 7, 2017

[†]Department of Physics, Stevens Institute of Technology, Hoboken, New Jersey 07030, United States

[‡]Department of Chemical Engineering and Materials Science, Stevens Institute of Technology, Hoboken, New Jersey 07030, United States

[§]National Renewable Energy Laboratory, Golden, Colorado 80401, United States

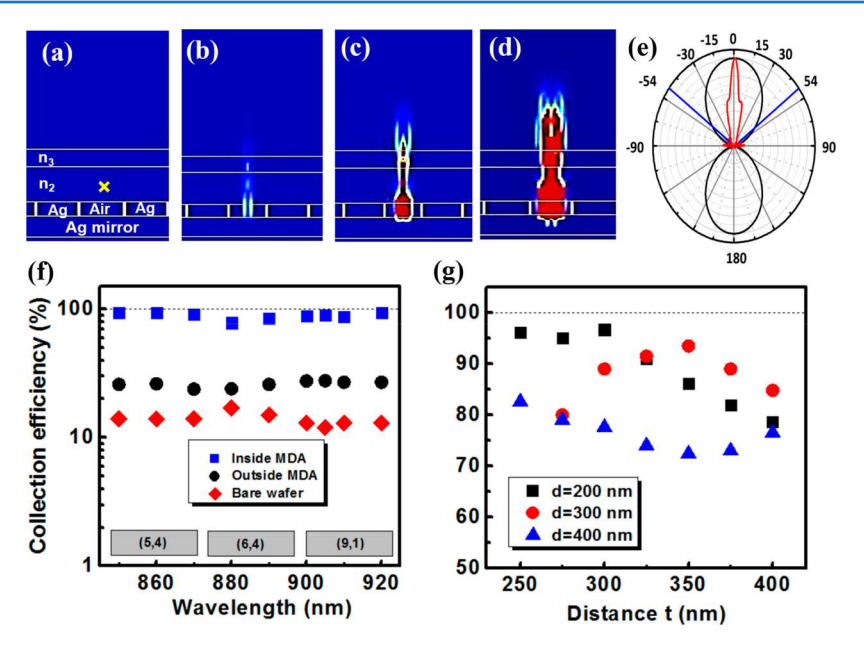


Figure 1. FDTD simulations of LCE for MDA cavities. (a) Schematic of the MDA cavity layer sequence. Yellow cross: SWCNT position. Lower medium $n_1 = 1$ (air), embedding medium $n_2 = 1.56$ (polystyrene), outcoupling medium $n_3 = 2.16$ (pentacene). (b-d) Temporal snapshots showing the development of the cavity mode on top of the air gap region. (e) Far-field emission profiles (emitted power density) of the MDA mode (red line) and a dipole emitter on a bare wafer (black line). Blue line: Light cone of objective (NA = 0.81). (f) Calculated LCE for dipole emitter positioned on bare wafer (red diamonds), outside MDA region (black circles), and inside MDA cavity (blue squares). Gray boxes: wavelength range of SWCNTs with (5,4), (6,4), and (9,1) chirality. (g) Calculated LCE at 860 nm as a function of distance t of the emitter from the outcoupling layer. Three cases are illustrated for different thickness d of the air-gap region.

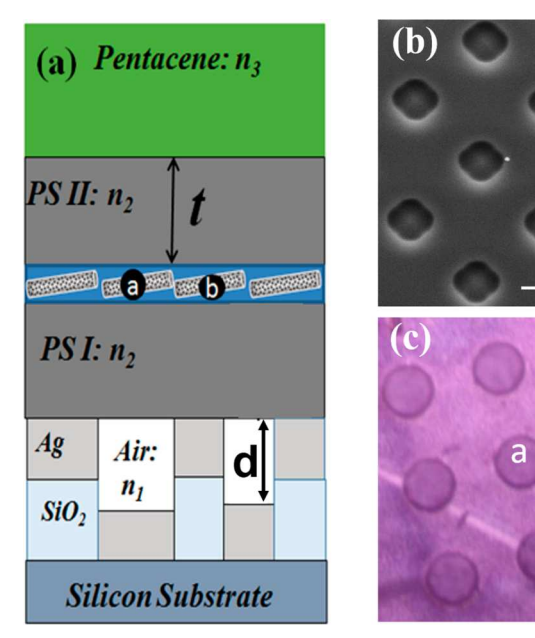
RESULTS

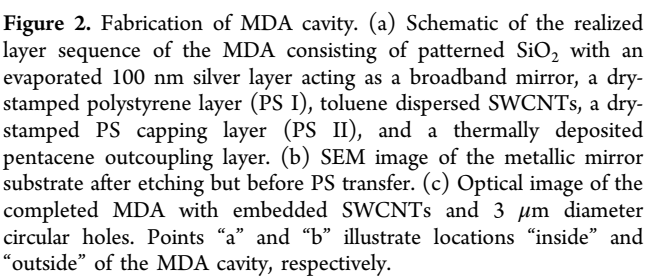
The basic principle to design a planar and broadband MDA that achieves near-unity LCE of embedded optical dipole emitters is given by the three-layer design rule $n_1 < n_2 < n_3$, introduced by Lee et al. ¹⁷ Here, n_1 is the refractive index of the lower medium (e.g., air) positioned on top of a metal mirror, n_2 is the medium embedding the dipole emitter, and n_3 is the photon extraction medium that interfaces to the far-field, as shown schematically in Figure 1a. We have set $n_2 = 1.56$ corresponding to polystyrene (PS) medium for the intermediate layer. This requirement reflects the need to prevent spectral diffusion and blinking of the SWCNT quantum emitter emission, which can be achieved via PS encapsulation. 13 To optimize the LCE we simulated the stack structure by varying the layer thicknesses and refractive indices n_1 and n_3 using the finite-difference time-domain (FDTD) method. The thickness of the lower medium d and the distance between dipole and output layer t are adjusted to maximize the cavity mode outcoupling and reduce the emission angle into the far-field. The resulting wave propagating dynamic of the MDA cavity mode real-time emission profile is shown in Figure 1b-d for three different timestamps. These near-field profiles inside the MDA structure illustrate that the electromagnetic field propagation is limited to the center region where $n_1 < n_2 <$ n_3 is fulfilled. The resulting far-field projection pattern of an embedded dipole emitter is shown in Figure 1e. Unlike the regular dipole emission pattern that emits half of the light in the wrong direction at a large emission angle of ±65°, the MDA mode emits solely into the upper half sphere, with a welldefined emission angle of ±15°. The emitted light from the MDA can thus be efficiently chip-to-fiber butt-coupled or, as in our case, collected into a microscope objective (NA = 0.81, collection angle $\pm 54^{\circ}$) without introducing additional losses.

The far-field LCE of the light emitted from the MDA mode can be calculated by integrating the collected power within the collection angle range of the objective. Figure 1f shows the resulting LCE values for the 900 nm band covering E₁₁ exciton emission from (5,4), (6,4), and (9,1) chirality SWCNTs and design parameters of d = 300 nm, t = 350 nm, $n_1 = 1$, $n_2 = 1.56$, and $n_3 = 2.0$ Collection efficiency near unity is achieved for emitters located inside the MDA cavity over the broad wavelength band covering 855-925 nm that is relevant in our study. Further outside of this bandwidth, the LCE drops down to about 80% for variations up to ±250 nm around 890 nm, illustrating the broadband enhancement provided by the MDA. Emitters located spatially outside the MDA mode but on the metal mirror are characterized by an average LCE = $26 \pm$ 1% and dipole emitters on bare wafers by LCE = $13 \pm 1\%$. Figure 1g shows that possible experimental variations in layer thickness t or SWCNT distance t + d from the metal mirror up to 100 nm result in about 25% reduction of the achievable LCE from unity. Best results are found with 97% for t = 300 nm and d = 200 nm, while 94% is found at our design parameters of t =350 nm and d = 300 nm that are experimentally easier to

Toward scalable fabrication of MDA structures, we note that n_1 should ideally be unity, which was previously achieved by approaching metal mirrors via external actuators to leave an air gap to the n_2 layer containing the emitter. ¹⁹ Since this approach is not easily scalable and requires off-chip actuators, we have directly embedded air gaps onto the wafer by using optical lithography to pattern silver mirrors with deep recesses based on etching 300 nm thick SiO_2 layers (see Supporting Information). Figure 2a shows a schematic of this design and Figure 2b is an example of the resulting silver mirror featuring an array of square shaped recesses with a 3 μ m side length and 300 nm depth. Since regular solution-based spin-coating

10 µm





techniques for subsequent PS layer deposition would refill these recesses to prevent air gap formation, we have employed here dry-stamping techniques typically utilized for assembly of heterostructures from 2D materials.²¹ Prefabricated PS layers

with targeted 350 nm thickness for PS I and 300 nm thickness for PS II were transferred via polymer release layers to assemble the cavity stack. To realize the high-index outcoupling layer, we have thermally evaporated a 250 nm pentacene layer. It was found that the thin-film pentacene layer displays polymorphism in the form of a low-index layer matching PS II and a high index layer forming the MDA cavity, resulting in an asymmetric configuration (see Supporting Information). Using all experimentally determined parameters, one can estimate via FDTD simulations an expected maximum LCE of 86% at 860 nm for these asymmetric conditions, which is slightly lower than the value determined for the symmetric structure (94%). Figure 2c shows an image of the fully assembled MDA stack featuring an array of circular air gaps with 3 μ m diameters. While our test structures containing MDA arrays were limited to areas of a few mm², the combination of photolithography and dry-transfer is a priori scalable to full wafer scale.

To demonstrate that SWCNT quantum emitters are located within the MDA cavity region and on top of the air gaps, that is, position "a" in Figure 2c, we recorded hyperspectral images of the E_{11} exciton emission from (5,4), (6,4), and (9,1) chirality tubes using band-pass filters, allowing only light in the 850-950 nm region toward the detector. These PL maps were recorded under 780 nm laser excitation, while samples were held at 3.8 K in an attodry1100 cryostat. 10 To reveal the outline of the MDAs air-gap region we separately recorded laser stray light reflected from the sample surface, as shown in Figure 3a,c,e,g. Outlines determined in this way were overlaid onto the hyperspectral PL maps shown in Figure 3b,d,f,h in form of dashed lines. Several MDA cavities are found that have a bright E₁₁ PL emission signature from an individual SWCNT located on top of the air gap region which in most cases is concentrated to a 1–2 μ m diameter area corresponding to the effective laser spot size. The spectra are characterized by a single sharp emission line indicative of a single quantum emitter. Cases where an individual SWCNT shows multiexciton localization

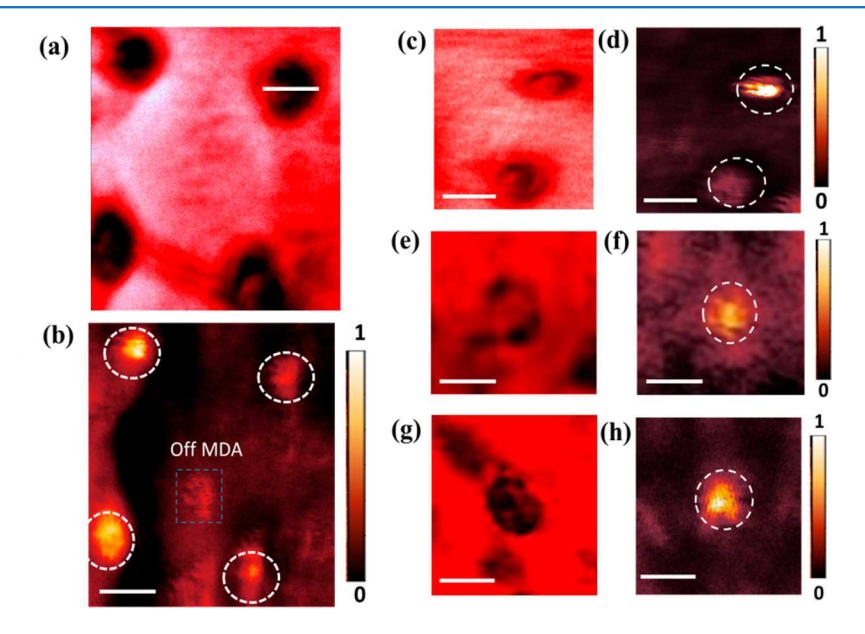


Figure 3. PL mapping of SWCNTs inside MDAs. (a, c, e, g) Spatial scans of back-reflected laser light illustrating the outline of the air gap regions forming the MDA cavity. (b, d, f, h) Corresponding hyperspectral images of same sample surface when laser stray light is blocked. Panels b and d have been spectrally filtered to capture the G-mode phonon as well as the exciton emission, that is, cover all SWCNTs. Panels f and h have been spectrally filtered on the exciton emission of (5,4) SWCNTs using a 10 nm bandpass filter over the ZPL. The white dashed circles trace the outline of the MDA region. The blue dashed square highlights an individual SWCNTs located spatially outside the MDA regions. Scale bar is 3 μ m.

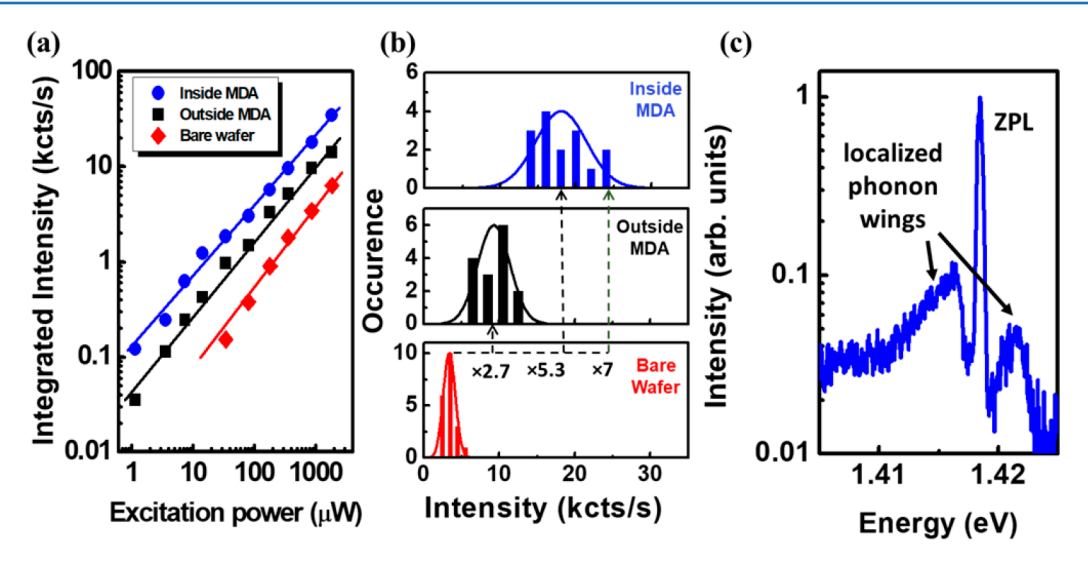


Figure 4. PL emission from individual SWCNTs located inside and outside of MDA. (a) Comparison of integrated PL intensity of the ZPL of the E₁₁ exciton emission from individual SWCNTs located inside the MDA (blue circles), outside the MDA (black squares), and on bare wafer (red diamonds). Intensity data are average values from 20 reference SWCNTs located on bare wafer, 15 SWCNTs outside the MDA, and 15 SWCNTs located inside the MDA structures. (b) Corresponding occurrence histograms for the three cases recorded at fixed pump power of 0.87 mW. The dashed lines highlight the average enhancement factors to the reference SWCNTs as well as the best case. (c) Normalized PL spectrum from individual SWCNTs located inside the MDA. ZPL at 1.418 eV is accompanied by the characteristic acoustic phonon wings for PFO-wrapped SWCNTs that have comparable magnitude to SWCNTs outside the MDA. All data are recorded at 3.8 K.

signatures, i.e. several spectrally separated lines in the E_{11} vicinity have been excluded here. Similar to our previous studies, 10,13 individual SWCNTs coupled to the MDA are characterized by pronounced single photon antibunching, with one example shown in Figure S2. A key advantage of the MDA is that the SWCNTs are not required to be located in the center of the MDA cavity. FDTD simulations show that LCE changes by only 4% when moving lateral over a 1.5 μ m distance along the MDA radius and is furthermore largely insensitive to lateral dipole orientation (see Figure S1). Figure 3b illustrates that bright emission also appears from emitters that are spatially off center.

The hyperspectral images show that individual SWCNTs can be located on top of the air gap where they can fully benefit from the large LCE of the MDA. To demonstrate this more quantitatively we investigated the PL intensity from 50 individual SWCNTs located either inside or outside the MDA structure, corresponding to locations a and b in Figure 2c, respectively, as well as reference SWCNTs located on bare wafers. Specifically, we recorded the integrated intensity of the zero-phonon-line (ZPL) of the E₁₁ exciton emission as a function of pump power for all three cases, as shown in Figure 4a. In all cases, a linear increase with pump power is observed, following the standard three-level rate equation analysis of 0D quantum-dot like excitons.²² The corresponding occurrence histograms in Figure 4b were recorded at fixed pump power of 0.87 mW for 15 tubes located over the air gap of the MDA, 15 tubes outside of the MDA, and 20 reference tubes on a bare wafer. Comparing the average reference tube intensity (3.4 kHz, variance 24%) to the average intensity of all tubes located over the MDA air gaps (18.1 kHz, variance 20%), a relative intensity enhancement factor (EF) of EF = 5.3 ± 1.3 is found. For the best case the intensity reaches up to 24 kHz corresponding to EF = 7. In contrast, SWCNTs located outside the MDA but on the planar metal mirror geometry display an average EF = 2.7 ± 0.6 . The relatively narrow intensity distribution of copolymer-wrapped SWCNTs is

comparable to our previous findings¹⁰ and makes it possible to quantitatively compare the LCE enhancement provided by the MDA. The fact that the variance of these PFO protected tubes is only 20–24% excludes a scenario where tube-to-tube variations can be responsible for the observed 5–7-fold intensity enhancement.

For quantitative comparison to the theory we note that EF has contributions from three processes, an enhanced absorption rate α , LCE enhancement ε , and a rate enhancement γ for the radiative emission due to the Purcell effect, resulting in EF \sim αεγ. Unlike high-Q cavities or plasmonic nanocavities, MDAs have a negligible Purcell effect since the quasi-waveguide mode is broadband $(Q \sim 1)$ while the mode volume is also very large. Similarly, α is found from FDTD to be ~15% by extracting the average electromagnetic field intensity enhancement resulting from the light concentration. Therefore, as a good approximation for MDA cavities one can consider the measured intensity EF to characterize directly the LCE enhancement. Recalling that the theoretical LCE = 13% at 860 nm for bare wafer location and LCE = 26% in location b away from the air gap (Figure 1f), one can predict EF = 2. Experimental values of $EF = 2.7 \pm 0.6$ for emitters outside the MDA match well to the theory. Likewise, FDTD theory predicts LCE= 86% in location a inside the MDA, limited by the presence of the thin-film phase in the pentacene layer, corresponding to a theoretical EF = 6.6. The experimentally determined average EF = 5.3 ± 1.3 (Figure 4b) in location a characterizes an average LCE of 69%, while the best case with EF = 7 reaches up to LCE = 92%. As a key result, coupling SWCNTs quantum emitters to MDA cavity modes results in near-unity LCE into spatially narrow (15°) output cones.

Beyond superior LCE the MDA has another advantage over approaches relying on high-Q dielectric cavities since it provides uniform broadband outcoupling without distorting the spectral line shape, thereby enabling efficient spectroscopy of single molecules. To illustrate this, we show in Figure 4c a typical spectrum of an individual SWCNT coupled to the

MDA. Beyond the E_{11} zero-phonon line (ZPL) acoustic-phonon wings are visible that are typical for copolymer-wrapped SWCNTs and have their origin in localization effects in the exciton—phonon interaction, as we demonstrated recently. The MDA can enhance both the phonon wings and the ZPL intensity uniformly over the ~ 10 nm wavelength range. In this case, the intensity of the low energy wing falls with 12% in the typical range of 15–22% that we have reported previously for PFO-wrapped SWCNTs. This contrasts with recent findings in high-Q dielectric cavities that strongly alter the relative coupling between ZPL and phonon wings. As a result, the MDA is an ideal platform to investigate exciton—phonon interactions at low light levels where pump-induced emitter dephasing is minimized.

In summary, we have designed on-chip arrays of MDAs that are tailored toward efficient light collection from embedded SWCNT quantum emitters by trapping air gaps on chip that form the cavity mode. The demonstrated 7-fold intensity enhancement when compared to SWCNTs located on bare wafers, corresponds to near-unity LCE up to 92% in the best case (average LCE of 69%) into a narrow output cone of $\pm 15^{\circ}$ enabling a priori fiber-to-chip butt coupling. In future work, one can also envision coupling quantum light emission from defect centers in 2D materials such as hBN²⁵ to realize efficient quantum light sources or spin-photon interfaces that require unity light collection to enable chip-scale quantum networks. The demonstrated polymer-film stacking via thermal release layers can also prevent the frequent solvent incompatibility issues when assembling organic optoelectronic devices.

ASSOCIATED CONTENT

S Supporting Information

The Supporting Information is available free of charge on the ACS Publications website at DOI: 10.1021/acsphotonics.7b00786.

Light collection efficiency as a function of dipole orientation. Fabrication procedure for metallo-dielectric antennas. Structural and optical properties of the pentacene layer. Photon correlation measurements showing single photon antibunching (PDF).

AUTHOR INFORMATION

Corresponding Author

*E-mail: strauf@stevens.edu.

ORCID

Yue Luo: 0000-0002-2757-5395

Jeffrey L. Blackburn: 0000-0002-9237-5891 Stephanie S. Lee: 0000-0003-0964-6353 Stefan Strauf: 0000-0002-9887-7059

Notes

The authors declare no competing financial interest.

ACKNOWLEDGMENTS

S.S. acknowledges financial support by the National Science Foundation (NSF) under Award DMR-1506711. S.S. and S.S.L. acknowledge financial support under NSF Award ECCS-MRI-1531237. J.B. and K.M. acknowledge funding from the Solar Photochemistry Program of the U.S. Department of Energy under Contract No. DE-AC36-08GO28308 to NREL.

REFERENCES

- (1) Högele, A.; Galland, C.; Winger, M.; Imamoğlu, A. Photon antibunching in the photoluminescence spectra of a single carbon nanotube. *Phys. Rev. Lett.* **2008**, *100*, 217401.
- (2) Sarpkaya, I.; Zhang, Z.; Walden-Newman, W.; Wang, X.; Hone, J.; Wong, C. W.; Strauf, S. Prolonged spontaneous emission and dephasing of localized excitons in air-bridged carbon nanotubes. *Nat. Commun.* **2012**, *4*, 2152.
- (3) Ma, X.; Hartmann, N. F.; Baldwin, J. K.; Doorn, S. K.; Htoon, H. Room-temperature single-photon generation from solitary dopants of carbon nanotubes. *Nat. Nanotechnol.* **2015**, *10*, *671*–*675*.
- (4) Ihly, R.; Mistry, K. S.; Ferguson, A. J.; Clikeman, T. T.; Larson, B. W.; Reid, O.; Boltalina, O. V.; Strauss, S. H.; Rumbles, G.; Blackburn, J. L. Tuning the driving force for exciton dissociation in single-walled carbon nanotube heterojunctions. *Nat. Chem.* **2016**, *8*, 603–609.
- (5) Diao, S.; Blackburn, J. L.; Hong, G.; Antaris, A. L.; Chang, J.; Wu, J. Z.; Zhang, B.; Cheng, K.; Kuo, C. J.; Dai, H. Fluorescence imaging in vivo at wavelengths beyond 1500 nm. *Angew. Chem.* **2015**, *127*, 14971–14975.
- (6) Nish, A.; Hwang, J. Y.; Doig, J.; Nicholas, R. J. Highly selective dispersion of single walled carbon nanotubes using aromatic polymers. *Nat. Nanotechnol.* **2007**, *2*, 640–646.
- (7) Lefebvre, J.; Austing, D. G.; Bond, J.; Finnie, P. Photoluminescence imaging of suspended single-walled carbon nanotubes. *Nano Lett.* **2006**, *6*, 1603–1608.
- (8) Akselrod, G. M.; Argyropoulos, C.; Hoang, T. B.; Ciracì, C.; Fang, C.; Huang, J.; Smith, D. R.; Mikkelsen, M. H. Probing the mechanisms of large Purcell enhancement in plasmonic nanoantennas. *Nat. Photonics* **2014**, *8*, 835–840.
- (9) Jeantet, A.; Chassagneux, Y.; Raynaud, C.; Roussignol, P.; Lauret, J. S.; Besga, B.; Estève, J.; Reichel, J.; Voisin, C. Widely tunable single-photon source from a carbon nanotube in the Purcell regime. *Phys. Rev. Lett.* **2016**, *116*, 247402.
- (10) Luo, Y.; Ahmadi, E. D.; Shayan, K.; Ma, Y.; Mistry, K. S.; Zhang, C.; Hone, J.; Blackburn, J. L.; Strauf, S. Near-unity quantum yield from carbon nanotube excitons coupled to plasmonic nanocavities. *Nat. Commun.* **2017**, *8*, 1413.
- (11) Ghosh, S.; Bachilo, S. M.; Weisman, R. B. Advanced sorting of single-walled carbon nanotubes by nonlinear density-gradient ultracentrifugation. *Nat. Nanotechnol.* **2010**, *5*, 443–450.
- (12) Koyama, K.; Yoshita, M.; Baba, M.; Suemoto, T.; Akiyama, H. High collection efficiency in fluorescence microscopy with a solid immersion lens. *Appl. Phys. Lett.* **1999**, *75*, 1667–1669.
- (13) Walden-Newman, W.; Sarpkaya, I.; Strauf, S. Quantum light signatures and nanosecond spectral diffusion from cavity-embedded carbon nanotubes. *Nano Lett.* **2012**, *12*, 1934—1941.
- (14) Wasey, J. A. E.; Barnes, W. L. Efficiency of spontaneous emission from planar microcavities. *J. Mod. Opt.* **2000**, *47*, 725–741.
- (15) Böhmler, M.; Hartmann, N.; Georgi, C.; Hennrich, F.; Green, A. A.; Hersam, M. C.; Hartschuh, A. Enhancing and redirecting carbon nanotube photoluminescence by an optical antenna. *Opt. Express* **2010**, *18*, 16443.
- (16) Barclay, P. E.; Srinivasan, K.; Borselli, M.; Painter, O. Efficient input and output fiber coupling to a photonic crystal waveguide. *Opt. Lett.* **2004**, *29*, 697–699.
- (17) Lee, K. G.; Chen, X. W.; Eghlidi, H.; Kukura, P.; Lettow, R.; Renn, A.; Sandoghdar, V.; Götzinger, S. A planar dielectric antenna for directional single-photon emission and near-unity collection efficiency. *Nat. Photonics* **2011**, *5*, 166–169.
- (18) Chen, W. X.; Agio, M.; Sandoghdar, V. Metallo-dielectric hybrid antennas for ultrastrong enhancement of spontaneous emission. *Phys. Rev. Lett.* **2012**, *108*, 233001.
- (19) Chu, X. L.; Brenner, T. J.; Chen, X. W.; Ghosh, Y.; Hollingsworth, J. A.; Sandoghdar, V.; Götzinger, S. Experimental realization of an optical antenna designed for collecting 99% of photons from a quantum emitter. *Optica* **2014**, *1*, 203–208.
- (20) Chu, X. L.; Götzinger, S.; Sandoghdar, V. A single molecule as a high-fidelity photon gun for producing intensity-squeezed light. *Nat. Photonics* **2016**, *11*, 58–62.

(21) Shepard, G. D.; Ajayi, O. A.; Li, X.; Zhu, X. Y.; Hone, J.; Strauf, S. Nanobubble induced formation of quantum emitters in monolayer semiconductors. 2D Mater. 2017, 4, 021019.

- (22) Hofmann, M. S.; Glückert, J. T.; Noé, J.; Bourjau, C.; Dehmel, R.; Högele, A. Bright, long-lived and coherent excitons in carbon nanotube quantum dots. *Nat. Nanotechnol.* **2013**, *8*, 502–505.
- (23) Sarpkaya, I.; Ahmadi, E. D.; Shepard, G. D.; Mistry, K. S.; Blackburn, J. L.; Strauf, S. Strong acoustic phonon localization in copolymer-wrapped carbon nanotubes. *ACS Nano* **2015**, *9*, 6383–6393.
- (24) Jeantet, A.; Chassagneux, Y.; Claude, T.; Roussignol, P.; Lauret, J. S.; Reichel, J.; Voisin, C. Exploiting one-dimensional exciton-phonon coupling for tunable and efficient single-photon generation with a carbon nanotube. *Nano Lett.* **2017**, *17*, 4184–4188.
- (25) Li, X.; Shepard, G. D.; Cupo, A.; Camporeale, N.; Shayan, K.; Luo, Y.; Meunier, V.; Strauf, S. Non-Magnetic Quantum Emitters in Boron Nitride with Ultra-Narrow and Sideband-Free Emission Spectra. ACS Nano 2017, 11, 6652–6660.